ELSEVIER

Journal of Nuclear Materials 290–293 (2001) 1123–1127

journal of nuclear materials

www.elsevier.nl/locate/jnucmat

Combined sheath and thermal analysis of overheated surfaces in fusion devices

D. Naujoks [a,*], J.N. Brooks [b]

[a] *Max-Planck-Institut für Plasmaphysik, EURATOM Association, Mohrenstrasse 40/41, D-10117 Berlin, Germany*
[b] *Argonne National Laboratory, 9700 S. Cass Avenu, Argonne, IL 60439, USA*

Abstract

The phenomenon of runaway surfaces overheating in fusion experiments due to plasma-sheath/surface-emission coupling has been analyzed. A semi-analytic model has been used as well as the BPHI-3D kinetic sheath code (J.N. Brooks, D. Naujoks, Phys. Plasmas 7 (2000) 2565) coupled with the THERM code which solves the non-stationary heat conduction equation also in 3D geometry. Runaway heating due to initial overheating and subsequent sheath breakdown and superheat has been analyzed for two materials – lithium and carbon. For typical liquid lithium divertor conditions the critical exposure time for thermal runaway is of order 10 ms – generally greater than plasma transient periods (e.g., ELMS) or flowing liquid exposure times. Critical exposure times for carbon are much longer (~1–2 s), as expected due to thermal property differences, and this may explain various 'hot spot' formations in carbon systems. It is also shown that, especially for carbon materials, effects such as flake formation and deterioration of heat conductivity can play a crucial role.

Keywords: Erosion; Redeposition; Plasma sheath; Plasma facing materials

1. Introduction

Localized overheated areas with dimension ~1 cm^2 have been observed on limiter and divertor plates in different tokamak experiments [2,3]. The surface temperatures measured by thermography have reached values above 2300°C. The resulting thermal sublimation of the material caused large influx of impurities into the edge plasma. In the case of oblique-incidence magnetic field geometry and high electron densities most of the slow-moving emitted material is ionized inside the magnetic sheath and immediately redeposited due to the strong sheath electric field. The resulting increased heat load can lead to runaway overheating and propagation of the hot areas over the surface. Thermal evaporation and sheath super-heat effects are also a particular concern with future planned liquid lithium surfaces (high vapor pressure) for fusion reactors.

2. Semi-analytic model

In [1], the newly developed BPHI-3D code has been used to calculate the change of potential and electric field inside the sheath and the in-sheath ionization/transport of emitted surface material as a function of the emitted flux. The enhancement of maximum heat load due to the lower sheath potential/higher electron flux, and the redeposited impurity ions is shown in Fig. 1 for a lithium target (3×8 cm^2) with a hot spot of diameter d. In these calculations, the ratio of emitted atom flux from the spot to the D–T ion flux to the target, $G = \Gamma_{\mathrm{Li}}/\Gamma_{\mathrm{DT}}$, is treated as a free parameter. The peak heat load, which is located near the central point of emission, depends upon the G ratio, the plasma parameters (electron density $n_e = 3 \times 10^{19}$ m^{-3}, electron temperature $T_e = 100$ eV) and the magnetic field geometry (oblique incidence, $\theta = 1.5°$, $B = 5$ T), also on the

* Corresponding author. Tel.: +49-30 20366 155; fax: +49-30 20366 111.
E-mail address: din@ipp.mpg.de (D. Naujoks).

0022-3115/01/$ - see front matter
PII: S0022-3115(00)00549-3

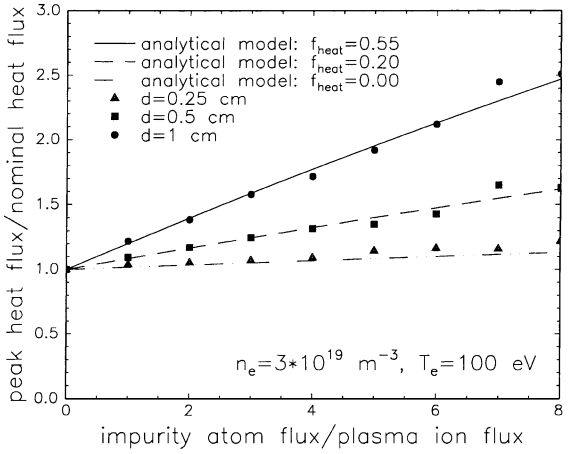

Fig. 1. The ratio of the maximum heat load $\max(P_{\rm pl}+P_{\rm imp})$ to the nominal heat load $P_{\rm pl}$ as a function of G for an emitting lithium spot of different diameters in comparison with analytical results. The used coefficients $f_{\rm heat}$ are indicated.

ratio of mean ionization length λ to spot radius r. With larger ionization lengths (and subsequently larger transport steps due to the emission–ionization–redeposition cycle) the excess heat load is distributed over larger areas. In order to describe this effect an additional factor $f_{\rm heat}\approx \pi r^2/(\pi[\max(\lambda,r)]^2)$ has been introduced in the analytical model presented in [1]. The heat flux due to in-sheath-ionized emitted atoms can then be estimated as

$$P_{\rm imp}=\Gamma_{\rm DT}Gf_{\rm redep}f_{\rm heat}f_{\rm pot}|e\phi_w|,$$

where the potential difference between the plasma and the material surface is described by [1]

$$e\phi_w\approx kT_{\rm e}\ln\left[4\frac{v_{\rm i}}{v_{\rm e}}\left(1+Gf_{\rm redep}f_{\rm geom}\right)\right],$$

where $v_{\rm i}$ is the ion sound speed and $v_{\rm e}$ is the thermal electron velocity. The 'nominal' heat load due to the impact of plasma ions and electrons onto surface is given by $P_{\rm pl}=\gamma kT_{\rm i}\Gamma_{\rm i}$ with the energy transmission coefficient [1]

$$\gamma=2+\frac{|e\phi_w|}{kT_{\rm e}}(1+Gf_{\rm redep}f_{\rm geom}f_{\rm pot})+2(1+Gf_wf_{\rm redep}f_{\rm geom}),$$

where $f_{\rm redep}$ serves to describe the complicated process of ionization and redeposition, $f_{\rm pot}$ the fraction of the sheath potential acquired by the redeposited impurity ions and $f_{\rm geom}$ is the ratio of the hot spot to the whole surface area under consideration.

The numerical results of the BPHI-3D calculations can be well described with the analytical model (Fig. 1) using parameters suggested by the code calculations. Therefore, it is used together with the numerical solution of the 1D heat conduction equation in a first attempt at a self-consistent analysis, i.e., to determine the emitted flux (G ratio) as a function of the surface temperature. The calculated heat flux due to plasma ions, electrons and impurity ions serves – in turn – as a boundary condition for the heat conduction equation, solution of which provides the surface temperature.

3. Lithium analysis

Fig. 2 shows the results for such an analysis. A 1-cm thick lithium layer with an initial temperature T_0 is heated due to the plasma impact ($n_{\rm e}=3\times10^{19}$ m^{-3}, $T_{\rm e}=100$ eV, $\theta=1.5°$ and the thermally emitted and then redeposited Li ions. Reaching a value of about 900 K (where $G\approx5$) the surface temperature $T_{\rm s}$ increases strongly due to the impact of more and more impurity ions and fast electrons. The parameters used in the calculations from BPHI-3D analysis [1], are $f_{\rm redep}=1.0$, $f_{\rm pot}=0.8, f_{\rm geom}=0.04, f_{\rm heat}=0.55$, atom density $\rho=534$ kg m^{-3}, heat capacity $c_{\rm p}=4160$ J kg^{-1} K^{-1}, heat conductivity $k=55$ W m^{-1}K^{-1}, sublimation flux $\Gamma_{\rm s}=2.63\times10^{24}\ P/\sqrt{6.939T_{\rm s}\ {\rm K}}$ atoms m^{-2} s^{-1}), vapor pressure $P=133.3\ \exp(18.4-18750/T_{\rm s}\ {\rm K})$ Pa. Cooling due to radiation, emission of atoms and electrons are taken into account.

Terminating the calculations upon reaching a G ratio of 10, a critical exposure time can be determined. This was done for different sets of plasma parameters (Fig. 3). The runaway exposure times are generally longer than the exposure times set by flow, which is encouraging.

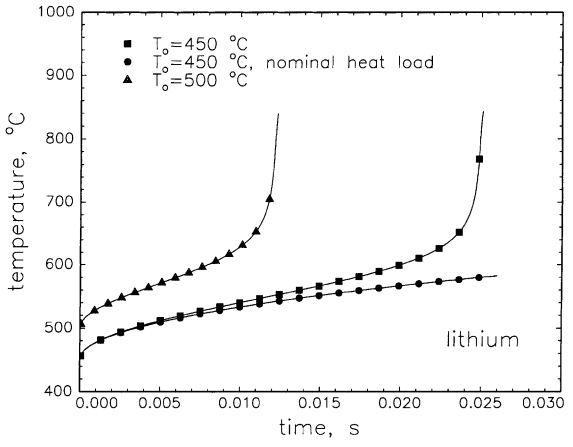

Fig. 2. Surface temperature of a lithium target $T_{\rm s}$ as a function of exposure time for two different starting temperatures T_0 (as indicated in the figure). For comparison, the change of $T_{\rm s}$ in time only due to 'nominal' heat load, i.e., without redeposition effect, is also shown.

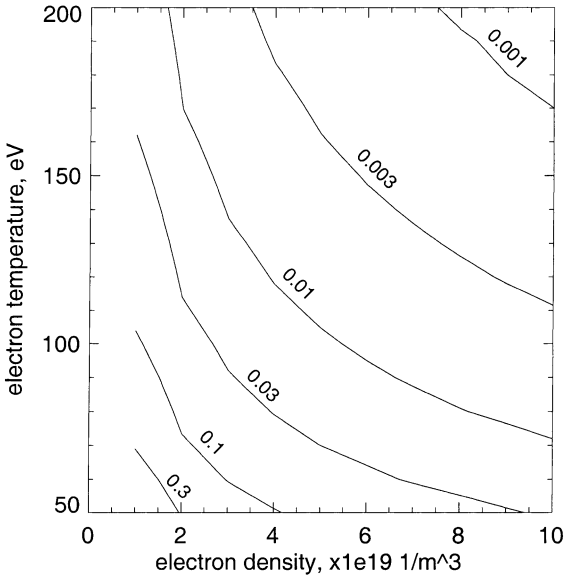

Fig. 3. Contours of critical exposure time t^* for a lithium target as a function of electron density and electron temperature ($T_0 = 450$°C. The values of t^* (in s) are indicated in the figure.

4. Carbon analysis

4.1. Semi-analytic results

Carbon sublimates at high rates only at very high surface temperatures as seen in Fig. 4. These are the results of a similar analysis as done for lithium. The parameters used are $n_e = 1 \times 10^{19}$ m^{-3}, $T_e = 50$ eV, $T_0 = 100$°C, $f_{redep} = 0.8$, $f_{pot} = 0.6$, $f_{geom} = 0.04$, $f_{heat} = 0.5$, thickness of carbon layer $\Delta z = 3$ cm, atom density

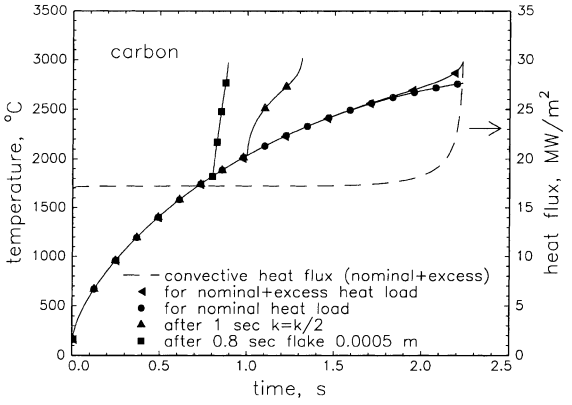

Fig. 4. Surface temperature of a carbon target as a function of exposure time for nominal and excess heat load. The results for two additional scenarios are also shown: (a) loss of heat contact due to flake formation with thickness of 500 μm at time $t = 0.8$ s; (b) deterioration of heat conductivity by a factor of two at $t = 1$ s.

$\rho = 1800$ kg m^{-3}, heat capacity $c_p = 1300$ J kg^{-1}K^{-1}, heat conductivity $k = [80\exp\{-0.002T(°C)\} + 30]$ W m^{-1} K^{-1}, sublimation flux $\Gamma_s = 2.5 \times 10^{24}$ $(T_s\ \mathrm{K})^{3.25} \exp(-7.4\ \mathrm{eV}/(kT_s\ \mathrm{K}))$ atoms m^{-2} s^{-1} [2]. Two possible scenarios (localized flake formation and deterioration of thermal properties) can lead to much lower critical surface temperatures. For one case, the convective heat load is also shown in Fig. 4. For an example that small particles can strongly contaminate the plasma, the number of atoms in a carbon cube with an edge length of about 450 μm is equal to the number of plasma ions in 1 m^3 of density $n_e = 1 \times 10^{19}$ m^{-3}.

4.2. BPHI-3D-THERM carbon analysis

A more realistic modeling can be achieved by coupling the BPHI-3D code with the THERM code. The latter program was initially developed to recalculate the heat flux from the surface temperature measured by means of the thermography diagnostics in the stellarator W7-AS. For this purpose, the non-stationary heat conduction equation is solved in full 3D geometry using the implicit alternating direction method based on the finite difference technique.

For the same plasma parameters as used in the semi-analytical model, a 1-cm thick carbon plate of dimension 2×2 cm^2 representing a typical portion of a carbon limiter, is considered. Starting with $T_0 = 100$°C the plate is heated due to plasma impact on the top. At the sides and the bottom (which are not exposed to the plasma) the heat flux and therefore, the gradient of the target temperature is fixed at zero as the boundary conditions. After 1 s an additional heat flux of 1/3 of the nominal heat load was assumed in the calculation. This artificial increase of heat load was restricted to a circular spot of diameter 0.5 cm located in the centre of the carbon plate. This models one possibility for hot spot initiation.

Fig. 5 shows the distribution of the heat flux at time 1.35 s, i.e., 0.35 s after the additional heat load starts to act. At this time the maximum heat flux is already shifted in the $E \times B$ direction due to the impact of emitted carbon atoms, which move after ionization in this direction.

The corresponding distribution of surface temperature is shown in Fig. 6. Shortly after this moment the surface temperature of the hot spot rises very strongly and a large amount of carbon is emitted into the plasma.

5. Discussion and summary

In this work, the sheath super-heat-transmission due to sheath breakdown and redeposition of thermally emitted material has been analyzed self-consistently. The analysis allows us to define critical exposure times for a lithium target under proposed lithium divertor design

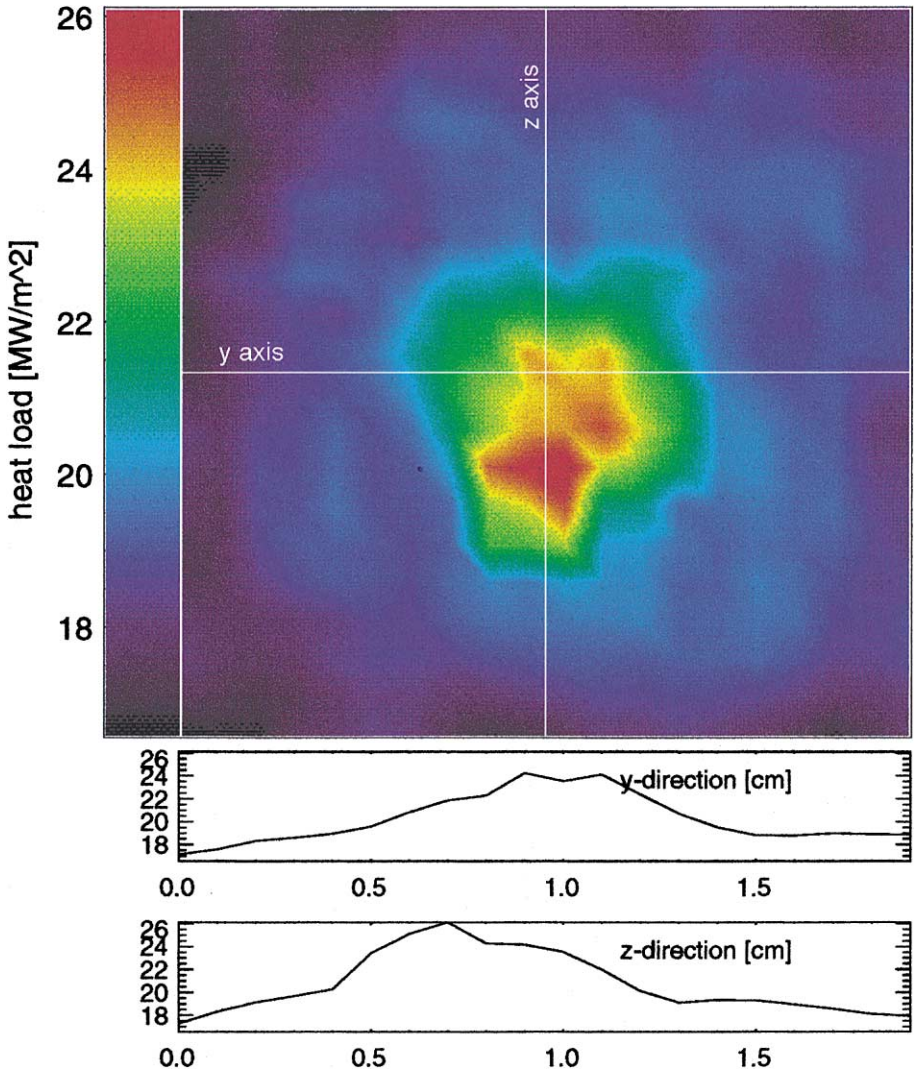

Fig. 5. Heat load distribution over the carbon target at time $t = 1.35$ s as calculated by BPHI-3D-THERM. The distribution along the indicated cross-hair are also shown.

conditions [4]. The calculated critical times are generally greater than flow exposure times, e.g., with a planned flow speed of about 10 m s^{-1} the exposure time can be reduced to 1 ms if 1 cm is taken for the width of the separatrix region. The results can also be used to estimate the allowed duration of transient plasma effects such as edge localized modes (ELMs) or vertical displacement events (VDEs).

Even for carbon with its exceptional thermal properties concerns remain if the heat conductivity deteriorates during the plasma exposure, e.g., due to the implantation of deuterium and the formation of a:C–H layers or due to the neutron bombardment. Flake formation or other effects of heat contact loss can be another reason for the hot spot phenomenon. It should be noted that the formation of flakes usually results in a 'leading edge', which worsens the problem. So active cooling of the plasma facing components as an appropriate method is needed to prevent overheating effects.

It should be noted that a possible change of plasma parameters, e.g., due to radiation cooling, as well as vapor shielding has not been taken into account. These effects are expected to be minor in the range of $0 < G < 10$ considered in this paper. Under these conditions, the impurity density in the sheath remains smaller than the electron density and the assumptions used are still valid.

The BPHI-3D-THERM modeling predicts the movement of the hot spot toward the $E \times B$ direction due to the movement of the impurity ions. But a detailed comparison with the observed movement in TEXTOR

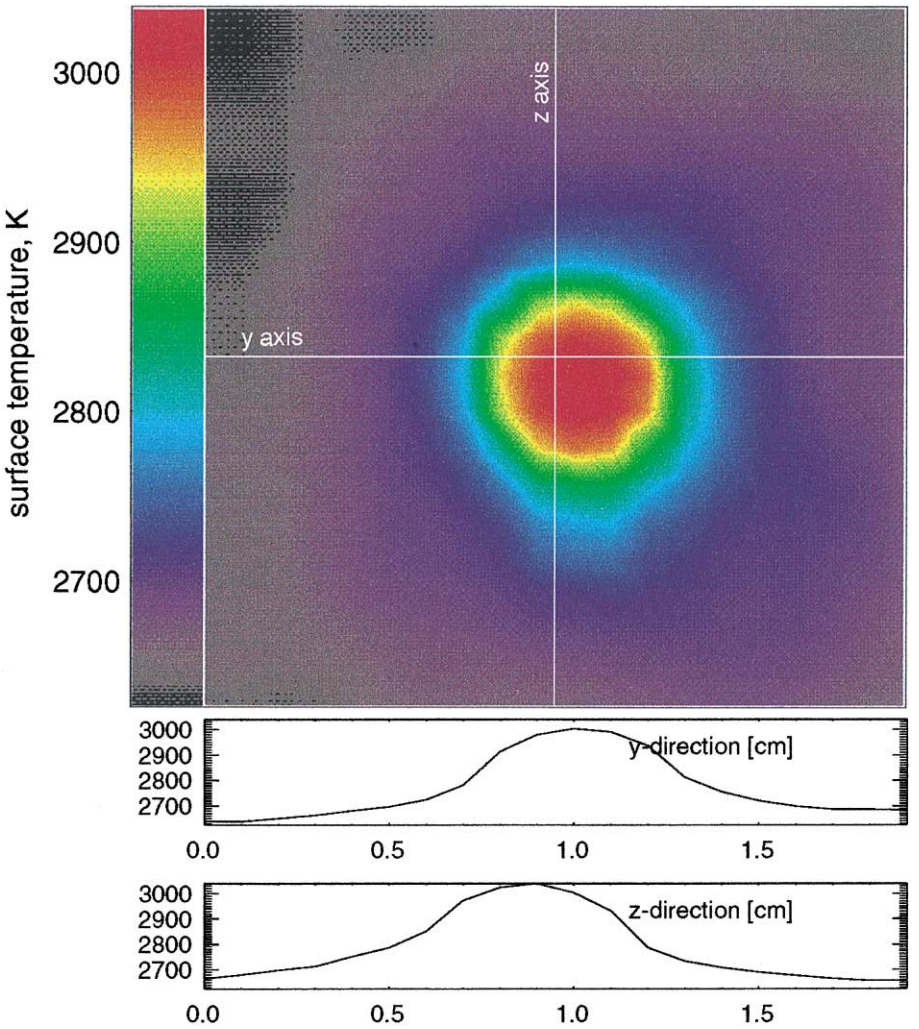

Fig. 6. Distribution of surface temperature over the carbon target at time $t = 1.35$ s as calculated by BPHI-3D-THERM.

[2] and the flame-like propagation in TORE SUPRA [3] still remain a challenge.

Thermionic electron emission does not act as strongly as in the 1D hot spot model of Tokar et al. [5] because of the relatively small areas of the hot spots with respect to the whole limiter/divertor plate. Of course, this is only valid in the case of conducting material, where the current balance is fulfilled for the whole plate and not only locally. For this case, the potential difference between the limiter/divertor plate and the plasma cannot be reduced to a value which is needed to explain the hot spot phenomenon of hot plasma electrons.

Acknowledgements

The work was supported by the US Department of Energy and by the European Commission under the Agreement for the Promotion of Staff Mobility, No. 131-83-7 FUSC. One of the authors (DN) would like to thank for the hospitality at the Argonne National Laboratory, where part of this work was performed.

References

[1] J.N. Brooks, D. Naujoks, Phys. Plasmas 7 (2000) 2565.
[2] V. Philipps, U. Samm, M.Z. Tokar, B. Unterberg, A. Pospieszczyk, B. Schweer, Nucl. Fus. 33 (1993) 953.
[3] D. Guilhem, A. Seigneur, P. Chappuis, et al., J. Nucl. Mater. 196–198 (1992) 759.
[4] J.N. Brooks, T. Ronglien, D.N. Ruzic, J.P. Allain, these Proceedings.
[5] M.Z. Tokar, A.V. Nedospasov, A.V. Yarochkin, Nucl. Fus. 32 (1992) 15.